

Degradation and Regeneration of n^+ -Doped Poly-Si Surface Passivation on p -Type and n -Type Cz-Si Under Illumination and Dark Annealing

Michael Winter , Stefan Bordihn , Robby Peibst , Rolf Brendel , and Jan Schmidt

Abstract—Degradation and regeneration of recombination parameters can occur in the bulk and at the surfaces of silicon solar cells. This article focuses on the time-resolved analysis of the recombination properties of textured 1.7 Ω cm boron-doped p -type Cz-Si and 5 Ω cm phosphorus-doped n -type Cz-Si wafers, where the surfaces are passivated by n^+ poly-Si on interfacial oxide layers exposed to a rapid thermal annealing (RTA) step in a conventional firing furnace. We observe a thermally activated instability in the lifetime over the entire examined injection range. Our experiments show that minority carrier injection (e.g., by illumination) is not required. Degradation in the surface passivation quality of the poly-Si on oxide layer—corresponding to an increase of the saturation current density J_0 by up to a factor of five—causes the degradation of the effective lifetime. Interestingly, the surface passivation fully regenerates under prolonged annealing and finally improves even beyond the initial state. Both the extent of the lifetime degradation and the change in J_0 depend on the postprocessing treatment temperature which we varied between 80 and 400 °C. Our results indicate that two different processes are responsible for the degradation and the regeneration. Reference samples which did not receive an RTA treatment show no degradation of the surface passivation quality. The RTA treatment applied therefore triggers the degradation effect. A large improvement of the surface passivation quality under prolonged annealing (e.g., at 400 °C) is observed for all samples examined in this study.

Index Terms—Carrier lifetime, degradation, poly-Si, Poly-Si on oxide (POLO), silicon, surface passivation.

Manuscript received August 30, 2019; revised October 24, 2019 and November 29, 2019; accepted December 21, 2019. This work was supported in part by the German State of Lower Saxony and in part by the European Union's Horizon 2020 Programme for research, technological developments, and demonstration within the research project DISC under Project 727529. (Corresponding author: Michael Winter.)

M. Winter, R. Brendel, and J. Schmidt are with the Institute for Solar Energy Research Hamelin/Emmerthal (ISFH), 31860 Emmerthal, Germany, and also with the Institute of Solid-State Physics, Leibniz University Hannover, 30167 Hannover, Germany (e-mail: m.winter@isfh.de; bren del@isfh.de; j.schmidt@isfh.de).

S. Bordihn is with the Institute for Solar Energy Research Hamelin/Emmerthal (ISFH), 31860 Emmerthal, Germany (e-mail: bordihn@isfh.de).

R. Peibst is with the Institute for Solar Energy Research Hamelin/Emmerthal (ISFH), 31860 Emmerthal, Germany, and also with the Institute of Electronic Materials and Devices, Leibniz University Hannover, 30167 Hannover, Germany (e-mail: peibst@isfh.de).

Color versions of one or more of the figures in this article are available online at <https://ieeexplore.ieee.org>.

Digital Object Identifier 10.1109/JPHOTOV.2020.2964987

I. INTRODUCTION

POLY-SI on oxide (POLO) layers have recently attracted great attention in the field of photovoltaic research, although first proposals to use them in solar cell production are much older [1]. Highly doped polycrystalline silicon layers on passivating interfacial oxide represent an advanced method to realize carrier-selective passivated contacts in high-efficiency silicon solar cells. It combines excellent passivation quality with saturation current densities (J_0) down to 0.6 fA/cm², as reported on planar test structures [2], [3], with very low-junction resistivities (0.6 mΩ cm² on n^+ POLO junctions) [4]. Outstanding energy conversion efficiencies of 26.1% for interdigitated back-contact solar cells [5], [6] and 25.8% for double-side-contacted solar cells have already been reported [6], [7]. Rapid thermal annealing (RTA) of POLO is highly relevant for the implementation of poly-Si-based passivating contacts into industrial-type solar cells with screen-printed and fired contacts [8], [9]. This article deals with possible instabilities of the silicon bulk as well as the poly-Si-passivated surfaces that might be caused by an industrial-type firing step, which is already known to cause a series of other mostly bulk-related defects [10], [11]. So far, however, there are only a few studies that deal with the degradation and regeneration of the silicon surface passivation, e.g., for dielectric passivation [12], and in particular none regarding poly-Si-based surface passivation. In this article, we examine possible instabilities during illumination and dark annealing which might occur for such systems in the bulk as well as at the surfaces of the silicon wafers.

II. EXPERIMENTAL DETAILS

Symmetrical lifetime samples were processed on random-pyramid-textured 1.7 Ω cm boron-doped p -type Cz-Si and 5 Ω cm phosphorus-doped n -type Cz-Si wafers with an ozone-grown interfacial oxide layer (~1.6-nm thick) and 150 nm (on p -type wafers) or 50 nm (on n -type wafers) *in-situ* doped n^+ poly-Si layers on top deposited by low-pressure chemical vapor deposition (centrotherm international, E1200 LPCVD furnace). Please note that in fact amorphous silicon (a-Si) layers are deposited during LPCVD which are rearranged to poly-Si layers in a high-temperature (HT) step performed at ~900 °C for ~30 min in a nitrogen atmosphere. If not explicitly mentioned, this HT step is omitted in this article, which pursues the “firing only” approach as presented e.g., by Ingenito *et al.* [8]. The

Wafer	Wafer preparation (thermal history)	Hot plate treatments & duration
<i>p</i> -type	(a) $\text{Al}_2\text{O}_3 + \text{Anneal } 425^\circ\text{C } 15\text{ min}$	(1) Illuminated (1 sun) 185°C 1000 h (2) Dark anneal (DA) 200°C 1000 h
	(b) High temperature anneal 900°C (HT) 30 min	(3) Dark anneal (DA) 300°C , 20 h (4) Dark anneal (DA) 400°C , 3 h
<i>n</i> -type	(c) High temperature anneal 860°C (HT) 30 min	$1\text{ sun}, 80^\circ\text{C}$ 1000 h
	(d) $\text{Al}_2\text{O}_3 + \text{Anneal } 425^\circ\text{C } 15\text{ min}$	

Fig. 1. Diagram of the conducted experiments sorted by wafer material and thermal history defining the samples. All samples are passivated by n^+ poly Si on ozone-grown interfacial oxide. The HT step is carried out directly after deposition of a-Si, which is rearranged to poly-Si in the process. The additional capping layer of Al_2O_3 serves as a hydrogen source for interface passivation.

lifetime samples were capped by 10 nm Al_2O_3 films used as a possible hydrogen source for interface passivation [13], [14] deposited using plasma-assisted atomic layer deposition (Oxford Instruments, FlexAl). Both *p*- and *n*-type wafers were exposed afterwards to a low-temperature annealing step at 425°C (15 min). The entire stack therefore consists of c-Si/ SiO_2 /poly-Si/ Al_2O_3 . The *p*-type Si wafers received an RTA treatment at 800°C set-peak temperature and a belt speed of 7 m/min in an industrial conveyor-belt firing furnace (centrotherm international, DO-FF-8.600-300). The *n*-type Si wafers were subdivided into four different groups and exposed to different temperature steps: (a) rapid thermal annealing at 800°C set-peak temperature at a belt speed of 7 m/min (referred to as RTA-samples), (b) a HT step at 900°C for 30 min in a quartz-tube furnace performed directly after LPCVD a-Si deposition, and (c) a high-temperature step at 860°C for 30 min after a-Si deposition plus an RTA step at 800°C at a belt speed of 7 m/min (HT+RTA). The *n*-type Si wafers which received no additional treatment in addition to the low-temperature annealing step at 425°C for 15 min serve as a reference [(d), annealed]. After sample processing, we applied two different experimental conditions: (i) exposure to a 100 mW/cm^2 (≤ 1 sun) halogen-lamp at a temperature of 185°C , and (ii) dark-annealing at three temperatures (200, 300, and 400°C) on a hot-plate in ambient environment. Most of the samples annealed in the dark were subsequently illuminated at 80°C and 1 sun. A graphical representation of the experiments can be found in Fig. 1.

For our experiments, the processed wafers are cut into $5\text{ cm} \times 5\text{ cm}$ samples using a laser process. The effective carrier lifetime τ_{eff} is measured as a function of the excess carrier density Δn at $\sim 30^\circ\text{C}$ using a WCT-120 lifetime tester from Sinton Instruments. The $\tau_{\text{eff}}(\Delta n)$ evolution of the *p*-type samples is analyzed at different Δn values between $2 \times 10^{14}\text{ cm}^{-3}$ and $3 \times 10^{16}\text{ cm}^{-3}$ to discriminate between bulk and surface recombination. The effective carrier lifetime of the *n*-type samples is analyzed at a fixed excess carrier concentration of $\Delta n = 1 \times 10^{15}\text{ cm}^{-3}$. Additionally, the entire injection dependence is examined at selected points in time. Both, the photoconductance decay and the quasi-steady-state photoconductance method were used to measure $\tau_{\text{eff}}(\Delta n)$ over a broad Δn range. In addition, the saturation current density J_0 —that represents

the surface passivation quality—is determined for all samples using the Kane and Swanson approach [15].

III. EXPERIMENTAL RESULTS AND DISCUSSION

A. Surface Passivation Quality of Fired *p*-type Cz-Si Lifetime Samples

In Fig. 2, the lifetime evolution of $1.7\Omega\text{ cm}$ boron-doped *p*-type Cz-Si samples is depicted for different Δn values to display the recombination properties at various injection conditions. Fig. 2(a) shows the effective lifetime τ_{eff} as a function of the cumulative exposure time to 1 sun at 185°C . At the low injection levels, two consecutive degradation and regeneration cycles can be observed on different time scales, whereas at the higher injection level of $\Delta n = 3 \times 10^{16}\text{ cm}^{-3}$ only one degradation/regeneration cycle is observed. The initial fast degradation (visible in the low injection curves) is completed after 0.01 h and its full regeneration after 0.1 h. This very fast degradation/regeneration cycle can be attributed to the boron–oxygen (BO) defect known from the literature [16], [17]. The subsequent second degradation process reaches a minimum lifetime value after ~ 30 h for all injection levels. The relatively flat injection-level dependence of the lifetime in the degraded state at low injection levels [Fig. 2(a) and (b)], degraded lifetimes at $\Delta n = 2 \times 10^{14}\text{ cm}^{-3}$ and $\Delta n = 1 \times 10^{15}\text{ cm}^{-3}$ are almost identical] and the fact that at high injection levels, the degradation is most pronounced points toward a degradation in the surface passivation quality. This is supported by the evolution of the saturation current density J_0 which increases by a factor of ~ 4.4 , as shown in the Fig. 2(c) and (d). J_0 was extracted at injection densities larger than $1 \times 10^{16}\text{ cm}^{-3}$. Continuing the illumination at 185°C [Fig. 2(a)] leads to a complete regeneration of the surface passivation, saturating at significantly lower J_0 values than in the initial state. In Fig. 2(b), τ_{eff} is shown for a sample after annealing at 200°C in the dark. The initial lifetime degradation/regeneration associated with the BO bulk defect is not observed in the dark annealing experiment, which is consistent with the well-known fact that the BO defect activation needs electron injection (e.g., by illumination). Interestingly, the second degradation and regeneration cycle occurs in the same way in the dark and under illumination. We thus conclude that

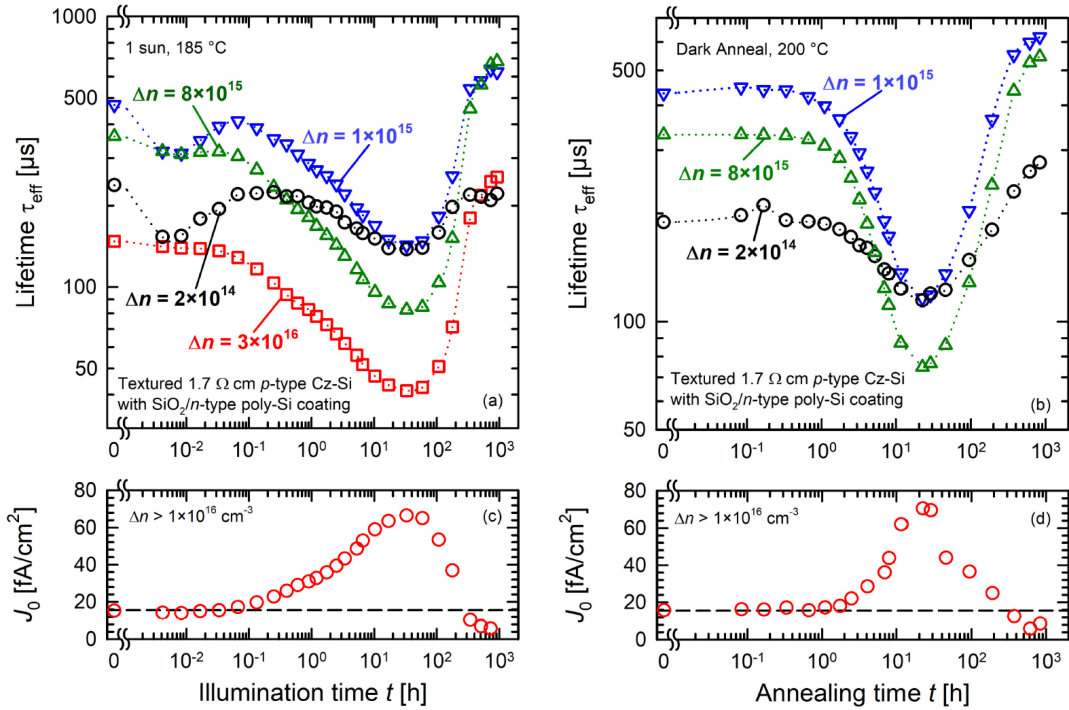


Fig. 2. Effective carrier lifetime τ_{eff} of poly-Si-passivated *p*-type Cz-Si samples extracted at different excess carrier densities Δn shown as a function of the cumulative exposure time. The sample shown in (a) is illuminated at 1 sun at 185 °C and the sample in (b) is annealed in the dark at 200 °C. The graphs (c) and (d) show the change of the saturation current density J_0 , extracted from the injection-dependent lifetime at high injection densities ($\geq 10^{16} \text{ cm}^{-3}$) using the Kane and Swanson method [15]. The dashed lines represent the initial J_0 value in order to illustrate the improvement in J_0 beyond the initial state through prolonged annealing.

the second surface-related degradation/regeneration cycle is a purely thermal process. From a practical point of view, our results demonstrate that a simple low-temperature anneal in the dark is sufficient to cure the fired poly-Si surface passivation and to obtain J_0 values $< 10 \text{ fA/cm}^2$ after firing.

Although the results of only one experiment are shown here, other *p*-type Si wafers were exposed to higher firing temperatures (up to 880 °C set-peak temperature) and/or other furnace belt speeds (4–7 m/min) and show comparable results.

Note that a surface-related degradation/regeneration effect is also observed on the examined 5 Ω cm phosphorus-doped *n*-type Cz-Si material (not shown here). The J_0 values extracted at $\Delta n \sim 8 \times 10^{15} \text{ cm}^{-3}$ change by a factor of ∼2.7 from 49 fA/cm² to 132 fA/cm² during degradation under 1 sun at 185 °C. Because of the significantly lower degradation and regeneration rate (by a factor of ∼6) of the surface-related effect on the examined *n*-type material, the experiment with the *n*-type Cz-Si samples was aborted. Instead, the effect is characterized further at higher temperatures in the Sections III-B and III-C.

B. Impact of Thermal History

Different types of lifetime samples of *p*- and *n*-type Cz-Si wafers were annealed in the dark at 300 °C [Fig. 3(a)] and illuminated afterwards at 1 sun and 80 °C [Fig. 3(b)] to compare the evolution of the surface passivation quality under accelerated conditions. The fired boron-doped Cz-Si sample (“*p*-type, RTA,” black circles) is cut from the same wafer as the samples discussed

in Section III-A. The surface-related degradation/regeneration cycle visible in Fig. 3(a) is clearly accelerated using the increased dark annealing temperature of 300 °C. In addition, the extent of the lifetime degradation is much smaller at the higher annealing temperature as is the increase in J_0 by a factor of only ∼1.5 [Fig. 3(c), black circles]. The saturated level of J_0 after prolonged annealing, however, is comparable to the results obtained in Section III-A, i.e., $< 10 \text{ fA/cm}^2$.

A similar, most likely surface-related effect can be observed on *n*-type Cz-Si samples fired at the same conditions as the *p*-type samples [Fig. 3(a), “*n*-type RTA”, blue inverse triangles]. The saturation current density J_0 increases by a factor of ∼1.7 [Fig. 3(c), blue inverse triangles, extracted at $\Delta n = 8 \times 10^{15} \text{ cm}^{-3}$] during degradation of the lifetime within the first hour of dark annealing. After the degradation, a regeneration of the lifetime to a level higher than the initial value is visible in Fig. 3(a). At 300 °C, the regeneration takes ∼20 h and the saturated J_0 value after regeneration amounts to 19 fA/cm², an improvement by a factor of ∼2.5 compared to the initial state.

Since the thermally activated surface-related effect is not only accelerated but also considerably reduced in its extent at higher annealing temperatures for both *p*- and *n*-type Si samples, two independent, parallel processes are responsible for the observed surface-related degradation and regeneration.

The same experiment is also conducted for similar *n*-type Si samples with different thermal histories. Whereas one sample in Fig. 3(a) received the high-temperature step at 900 °C for 30 min (“*n*-type, HT,” green triangles), which is commonly used

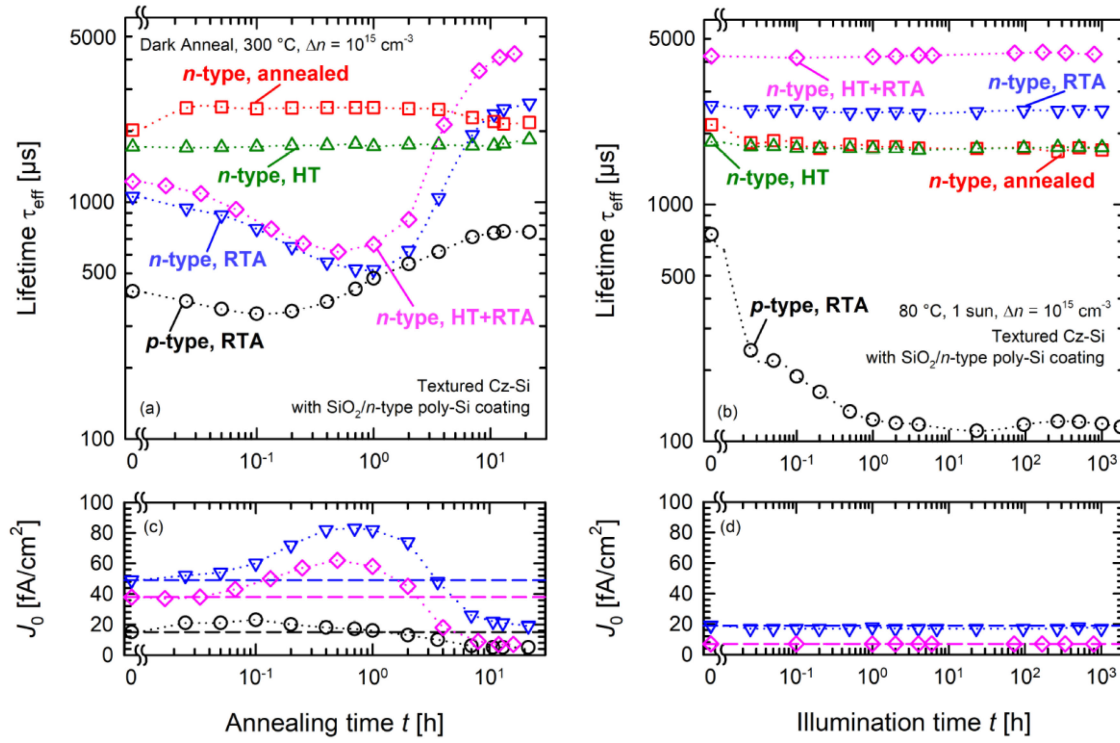


Fig. 3. Effective carrier lifetime τ_{eff} extracted at $\Delta n = 10^{15} \text{ cm}^{-3}$ as a function of the cumulative exposure times for p - and n -type Cz-Si samples. (a) Five lifetime samples with different thermal history annealed in the dark at 300°C . (b) The same lifetime samples illuminated afterwards at 1 sun and 80°C . The graphs (c) and (d) show the simultaneous change of the saturation current densities J_0 , extracted from the injection-dependent lifetime at high injection densities ($\geq 1 \times 10^{16} \text{ cm}^{-3}$ for p -type, $\geq 8 \times 10^{15} \text{ cm}^{-3}$ for n -type Si samples). The symbols and colours used match the corresponding graphs in (a) and (b). The dashed lines represent the initial J_0 values to illustrate the improvement under prolonged annealing (c) and the stability of the surface passivation quality under illumination (d).

to rearrange the deposited a-Si layers to poly Si layers [18], another sample was only annealed at 425°C for 15 min without any further annealing step (“ n -type, annealed,” red squares). Neither of the two samples shows a degradation of the lifetime as observed for the fired samples. Please note, however, that for the HT sample, a slight improvement in J_0 from 25 to 21 fA/cm² is observed, whereas J_0 for the annealed sample remains stable at 13 fA/cm² [both not shown in Fig. 3(c)]. Finally, the last sample shown in Fig. 3(a) received both an HT treatment and a subsequent RTA step (“ n -type, HT+RTA,” pink diamonds). The same degradation of the surface passivation quality as for all other fired samples is visible. The saturation current density increases by a factor of ~ 1.9 [Fig. 3(c), pink diamonds]. The subsequent regeneration results in a significantly higher lifetime caused by an improvement of the surface passivation quality by a factor of more than 5 to $J_0 = 7 \text{ fA/cm}^2$ compared to the initial state after firing. The RTA and the HT+RTA samples show a very similar behavior of the surface-related degradation effect. Note, however, that for the RTA sample the “poly-Si” layer is mostly in its amorphous state because the thermal budget is not sufficient to fully crystallize the a-Si layer during the ultrafast thermal step. Therefore, since the structure of the poly-Si is very different for both samples, we assume that hydrogen passivation of the dangling bonds at the Si-SiO₂ interface is responsible for the observed interface-related effects. There are similar investigations by Sperber *et al.* for dielectric passivation [19].

A subsequent illumination of all samples at 1 sun and 80°C serves to test the stability of the surface passivation quality. The results are shown in Fig. 3(b). The lifetime values of the n -type samples remain fully stable up to the maximum applied exposure time of over 1000 h [as do the corresponding J_0 values, see Fig. 3(d)]. The p -type Cz-Si sample, however, degrades in agreement with the bulk-related activation of the BO defect. The J_0 value after completion of the experiment is 7 fA/cm². Please note that no subsequent regeneration of the lifetime is observed within the duration of the experiment (almost 2000 h at 80°C). However, we were able to deactivate the BO defect again by dark annealing at 200°C for 10 min [20], [21]. The injection-dependent lifetime afterwards is virtually identical to the lifetime measured before illumination. We conclude that the surface-related improvement is not affected by the additional dark anneal.

C. Effect of Increased Annealing Temperature

The surface passivation quality improves for fired p - and n -type Cz-Si samples and, consequently, so does the lifetime over a broad injection range under prolonged annealing at elevated temperatures. Therefore, the surface passivation depends on the thermal history of the sample. To examine this further, the dark annealing temperature was increased to 400°C . The measured lifetime evolutions are shown in Fig. 4(a). The surface-related degradation discussed in Sections III-A and III-B is not visible

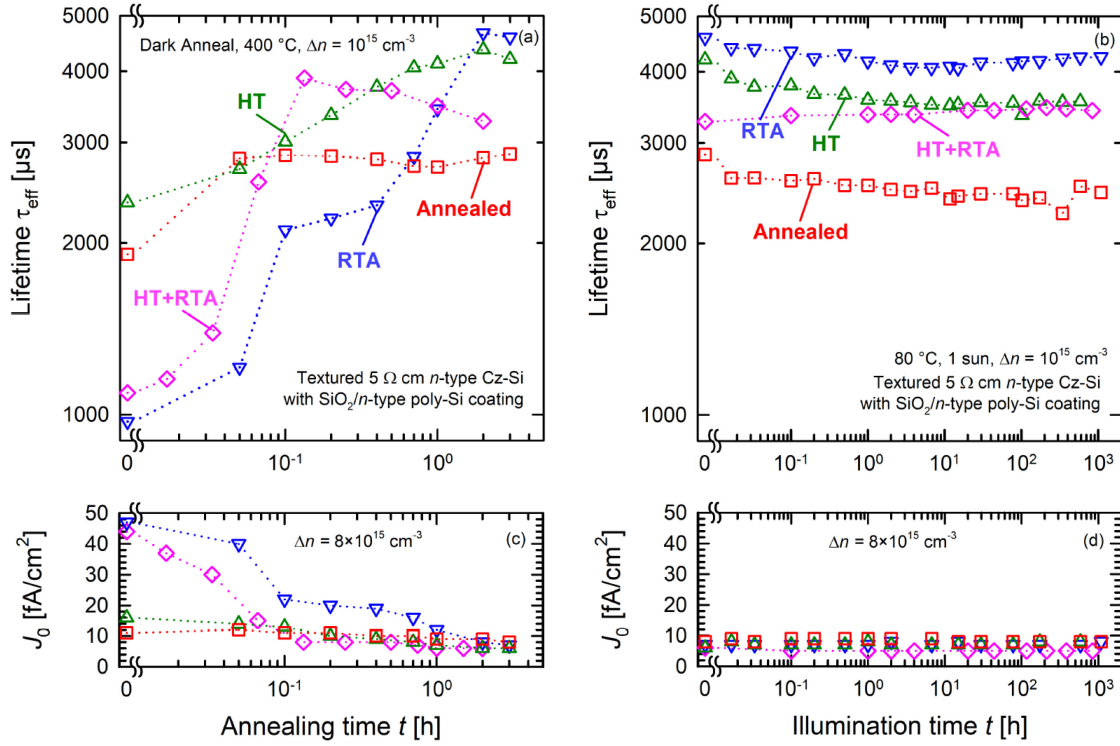


Fig. 4. Effective carrier lifetime τ_{eff} extracted at $\Delta n = 10^{15} \text{ cm}^{-3}$ as a function of the cumulative exposure times. (a) Four n -type lifetime samples with different thermal history are annealed in the dark at 400 °C. (b) The same lifetime samples are illuminated afterwards at 1 sun and 80 °C. The graphs (c) and (d) show the simultaneous change of the saturation current density J_0 , extracted from the injection-dependent lifetime at high injection densities ($8 \times 10^{15} \text{ cm}^{-3}$). The symbols and colours used match the corresponding graphs in (a) and (b).

anymore at the higher annealing temperature of 400 °C. The focus of this experiment, however, is on the improvement of the surface passivation quality. Indeed, we observe an increase of the lifetime, for some samples (RTA and HT) even beyond the level already observed in Section III-B. There is also a significant improvement visible for the HT-sample (green triangles), which was not observed at 300 °C annealing temperature and is possibly related to the early termination of the experiment. The increasing lifetime during annealing can be attributed to a further improvement of the surface passivation quality probably due to a further hydrogenation of the Si-SiO₂ interface. This is represented by an additional reduction of the saturation current density J_0 by a factor of ~2 compared to Section III-B. For all examined samples, J_0 values in the range between 5 and 8 fA/cm² are obtained. However, neither the fast improvement of the annealed sample after 3 min at 400 °C [Fig. 4(a), red squares] nor the small reduction in lifetime of the HT+RTA sample after 10 min at 400 °C [Fig. 4(a), pink diamonds] can be attributed to a change of the surface passivation quality, as shown in Fig. 4(c). The cause for these two effects is rather to be found at low injection levels and will be discussed in Fig. 5.

The subsequent illumination at 80 °C shown in Fig. 4(b) reveals for most samples a decrease in lifetime at $\Delta n = 10^{15} \text{ cm}^{-3}$. Nevertheless, the lifetime remains stable at a higher level than obtained in Section III-B without any change in the corresponding J_0 values.

Fig. 5 shows the injection dependent effective lifetimes of the four n -type samples shown in Fig. 4. For each sample, the initial lifetime after respective processing (black circles), the highest lifetime (measured at $\Delta n = 10^{15} \text{ cm}^{-3}$) after annealing in the dark at 400 °C (blue inverse triangles), and the lifetime after illumination at 80 °C and 1 sun for up to 1000 h (red squares) are shown. A lifetime improvement over the entire examined injection range is clearly visible for all samples. The lifetime changes of the sample, annealed during processing [Fig. 5(b)], could be explained by an additional iron gettering effect [22]–[24]. The improvement of the fired [RTA, Fig. 5(a)], the high-temperature-annealed [HT, Fig. 5(c)], and the sample which received both the HT- and the RTA treatment [Fig. 5(d)] can only be understood by a significant improvement of the surface passivation quality. The degradation of the effective lifetime of the HT+RTA sample after 10 min at 400 °C [Fig. 4(a), pink diamonds] is only present at low injection levels. The lifetime at higher injection levels (and consequently J_0) improves further as seen in comparison of pink diamonds in Fig. 4(c) and blue inverse triangles as well as red squares in Fig. 5(d). The decrease of the lifetime for almost all samples [Fig. 4(b)] under long-term illumination at 80 °C is mainly limited to the low injection levels (compare Fig. 5, red squares), which indicates some instabilities in the bulk lifetime of our samples. The high-injection lifetime and the corresponding J_0 value remain unchanged, i.e., the surface passivation quality has reached a stable level.

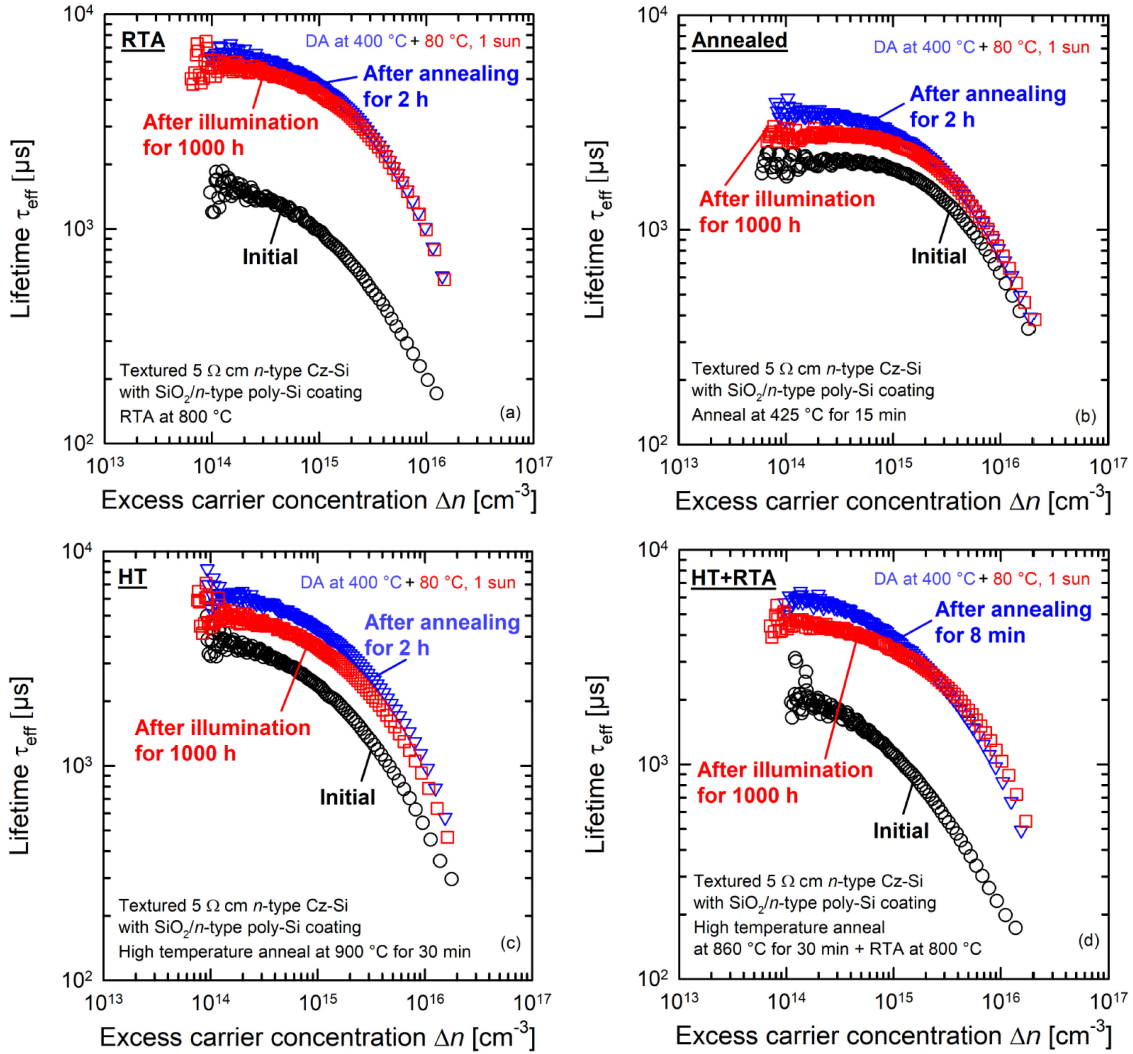


Fig. 5. Injection dependent effective lifetime for the four *n*-type samples is shown in Fig. 4. Each sample has a different defining step during processing: (a) RTA at 800 °C, (b) anneal at 425 °C for 15 min, (c) high temperature anneal at 900 °C for 30 min, (d) high-temperature anneal at 860 °C for 30 min followed by an RTA treatment at 800 °C. The initial lifetime (black circles) represents the state of the samples after processing. Afterwards, the samples are annealed in the dark at 400 °C for up to several hours. The injection dependent lifetime with the highest value measured at $\Delta n = 1 \times 10^{15} \text{ cm}^{-3}$ in Fig. 4(a) is shown in each case (blue inverse triangles). The red squares represent the state of the samples after illumination at 80 °C and 1 sun for up to 1000 h.

The improvement of the surface passivation quality can be achieved under illumination at the same temperature as it was observed during dark annealing, that results in the same characteristics as described in this Section III-C.

IV. CONCLUSION

In this article, we performed a series of carrier lifetime experiments after annealing at elevated temperatures under illumination and in the dark to examine possible instabilities of the bulk as well as of the surface passivation quality. Our samples were symmetrically processed random-pyramid-textured *p*- and *n*-type Cz-Si samples passivated by n^+ poly-Si on interfacial oxide layers. We observed lifetime instability on all examined samples after an industrial-type firing step, which we attribute to a degradation of the surface passivation quality. The degradation was followed by a regeneration of the lifetime to a level beyond

the initial state under prolonged annealing. Please note that we do not expect a change of the junction resistivity by our post-processing annealing treatments because the temperatures are too low to change the crystal structure of our poly-Si layers or to increase the in-diffusion of dopant atoms from the poly-Si layer into the crystalline silicon. We can also exclude an additional growth of the interfacial oxide layer as we do not expect further oxygen diffusion to the interface nor that the RTA is sufficient for an additional oxide growth beyond the already existing $\sim 1.6 \text{ nm}$. Therefore, though we did not measure it, we expect the junction resistivity to be as low as previously published [4].

As the nonfired poly-Si layers show a good stability during low-temperature annealing [cf. Fig. 3(a)], the origin for the instability in the surface passivation quality for both *p*- and *n*-type Si samples was identified to be the firing step, which is attractive to replace the more time-consuming usual high-temperature treatment and to allow for the implementation of screen-printed

and fired contacts. The standard prolonged high-temperature treatment is performed much closer to a thermal equilibrium situation than a conveyor-belt furnace process, where in particular, the cooling is very fast. Therefore, the hydrogen passivation of the dangling bonds is most likely in a different configuration after RTA than after a conventional high-temperature process. Through prolonged annealing after firing, the configuration of the hydrogen passivation at the Si-SiO₂ interface changes further, which results first in a degradation and afterwards in an improvement of the surface passivation quality. We showed that a degradation of the surface passivation quality can also be observed on samples which received both the HT- and the RTA-treatment. We observed this effect even at low-treatment temperatures of 80 °C with a correspondingly low degradation rate (not shown in this contribution). We measured a significant improvement of the surface passivation quality manifesting itself under prolonged annealing at increased temperatures around 400 °C for all examined samples which received either HT or RTA treatments.

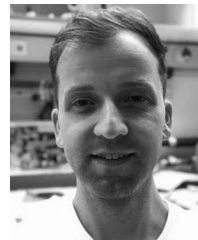
REFERENCES

- [1] J. Y. Gan and R. M. Swanson, "Polysilicon emitters for silicon concentrator solar cells," in *Proc. IEEE Conf. Photovolt. Spec.*, Kissimmee, FL, USA, 1990, pp. 245–250.
- [2] R. Peibst *et al.*, "Implementation of n+ and p+ poly junctions on front and rear side of double-side contacted industrial silicon solar cells," in *Proc. 32th Eur. Photovolt. Sol. Energy Conf. Exhib.*, Munich, Germany, 2016, pp. 323–327.
- [3] U. Römer *et al.*, "Ion implantation for poly-Si passivated back-junction back-contacted solar cells," *IEEE J. Photovolt.*, vol. 5, no. 2, pp. 507–514, Mar. 2015.
- [4] M. Rienacker *et al.*, "Junction resistivity of carrier-selective polysilicon on oxide junctions and its impact on solar cell performance," *IEEE J. Photovolt.*, vol. 7, no. 1, pp. 11–18, Jan. 2017.
- [5] F. Haase *et al.*, "Laser contact openings for local poly-Si-metal contacts enabling 26.1%-efficient POLO-IBC solar cells," *Sol. Energy Mater. Sol. Cells*, vol. 186, pp. 184–193, 2018.
- [6] M. A. Green *et al.*, "Solar cell efficiency tables (version 52)," *Prog. Photovolt. Res. Appl.*, vol. 26, no. 7, pp. 427–436, 2018.
- [7] A. Richter *et al.*, "n-Type Si solar cells with passivating electron contact: Identifying sources for efficiency limitations by wafer thickness and resistivity variation," *Sol. Energy Mater. Sol. Cells*, vol. 173, pp. 96–105, 2017.
- [8] A. Ingenito *et al.*, "A passivating contact for silicon solar cells formed during a single firing thermal annealing," *Nature Energy*, vol. 3, no. 9, pp. 800–808, 2018.
- [9] A. Merkle *et al.*, "Atmospheric pressure chemical vapor deposition of in-situ doped amorphous silicon layers for passivating contacts," in *Proc. 35th Eur. Photovolt. Sol. Energy Conf. Exhib.*, 2018, pp. 785–791.
- [10] D. Bredemeier, D. Walter, S. Herlufsen, and J. Schmidt, "Lifetime degradation and regeneration in multicrystalline silicon under illumination at elevated temperature," *AIP Adv.*, vol. 6, no. 3, 2016, Art. no. 35119.
- [11] D. Chen *et al.*, "Evidence of an identical firing-activated carrier-induced defect in monocrystalline and multicrystalline silicon," *Sol. Energy Mater. Sol. Cells*, vol. 172, pp. 293–300, 2017.
- [12] D. Sperber, A. Herguth, and G. Hahn, "Instability of dielectric surface passivation quality at elevated temperature and illumination," *Energy Procedia*, vol. 92, pp. 211–217, 2016.
- [13] B. Nemeth *et al.*, "Polycrystalline silicon passivated tunneling contacts for high efficiency silicon solar cells," *J. Mater. Res.*, vol. 31, no. 6, pp. 671–681, 2016.
- [14] A. Mewe *et al.*, "Full wafer size IBC cell with polysilicon passivating contacts," in *Proc. AIP Conf. Proc.*, Lausanne, Switzerland, 2018, pp. 1–4.
- [15] D. Kane and R. Swanson, "Measurement of the emitter saturation current by a contactless photoconductivity decay method," in *Proc. 18th IEEE Photovolt. Spec. Conf.*, 1985, pp. 579–583.
- [16] K. Bothe and J. Schmidt, "Electronically activated boron-oxygen-related recombination centers in crystalline silicon," *J. Appl. Phys.*, vol. 99, no. 1, 2006, Art. no. 13701.
- [17] J. Schmidt, "Light-induced degradation in crystalline silicon solar cells," *Solid State Phenomena*, vol. 95/96, pp. 187–196, 2004.
- [18] R. Peibst *et al.*, "A simple model describing the symmetric I-V characteristics of p polycrystalline Si/n Monocrystalline Si, and n polycrystalline Si/p Monocrystalline Si junctions," *IEEE J. Photovolt.*, vol. 4, no. 3, pp. 841–850, May 2014.
- [19] D. Sperber, A. Graf, D. Skorka, A. Herguth, and G. Hahn, "Degradation of surface passivation on crystalline silicon and its impact on light-induced degradation experiments," *IEEE J. Photovolt.*, vol. 7, no. 6, pp. 1627–1634, Nov. 2017.
- [20] H. Fischer and W. Pschunder, "Investigation of photon and thermal induced changes in silicon solar cells," in *Proc. 10th IEEE Photovolt. Spec. Conf.*, 1973, pp. 404–4011.
- [21] J. Schmidt, A. G. Aberle, and R. Hezel, "Investigation of carrier lifetime instabilities in CZ grown silicon," in *Proc. Rec. 26th IEEE Photovolt. Spec. Conf.*, 1997, pp. 13–18.
- [22] A. Y. Liu and D. Macdonald, "Impurity gettering effect of atomic layer deposited aluminum oxide films on silicon wafers," *Appl. Phys. Lett.*, vol. 110, no. 19, 2017, Art. no. 191604.
- [23] J. Krügener *et al.*, "Improvement of the SRH bulk lifetime upon formation of n-type POLO junctions for 25% efficient Si solar cells," *Sol. Energy Mater. Sol. Cells*, vol. 173, pp. 85–91, 2017.
- [24] C. Gemmel *et al.*, "9 ms carrier lifetime in kerfless epitaxial wafers by n-type POLO gettering," in *Proc. AIP Conf. Proc.*, Lausanne, Switzerland, 2018, pp. 1–7.



Michael Winter received the M.Sc. degree in physics from Leibniz University Hannover, Hannover, Germany in 2017. In 2018, he joined the Institute for Solar Energy Research, Hamelin, Germany, where he is currently working toward the Ph.D. degree in physics with the Photovoltaic Department.

His research interests include the light- and temperature-induced lifetime changes caused by effects in the bulk as well as at the surfaces of silicon-based photovoltaic materials.



Stefan Bordihn received the B.Sc. and M.Sc. degrees in renewable energy systems from the University of Applied Science, Berlin, Germany, in 2007 and 2010, respectively, and the Ph.D. degree from Hanwha Q Cells, Seoul, South Korea and the Eindhoven University of Technology, Eindhoven, The Netherlands, in the field of plasma-based thin film processing for the application in high-efficiency solar cells in 2014.

He worked as an Expert and Project Leader with Hanwha Q Cells until he joined the Institute for Solar Energy Research Hamelin, Germany, in 2018.



Robby Peibst received the Diploma in technical physics from the Technische Universität Ilmenau, Ilmenau, Germany, in 2005, and the Ph.D. degree in the field of microelectronics from the Leibniz University of Hannover, Hannover, Germany, in 2010.

In 2010, he joined the Institute for Solar Energy Research Hamelin, Germany, where he has been leading the group "Emerging Solar Cell Technologies" since 2013. Since 2016, he has been a Professor with the Leibniz University Hannover. His research interests include techniques for producing high-efficient silicon solar cells such as passivating contacts, silicon-based tandem cells, and special applications of photovoltaics.



Rolf Brendel studied in Freiburg and Heidelberg, Germany, and at the University of Sussex, Brighton, U.K. He received the Physics Diploma degree in nuclear fusion research in 1987, and the degree for school teaching in physics and mathematics in 1988, both from the Heidelberg University. He received the Ph.D. degree in infrared spectroscopy from the University of Erlangen, Erlangen, Germany, in 1992.

He then joined the Max-Planck-Institute for Solid State Research in Stuttgart to study the physics of thin-film silicon solar cells and the thermodynamics of photovoltaic power conversion. In 1997, he became the Head of the Division for Thermosensorics and Photovoltaics with the Bavarian Center for Applied Energy Research, Wuerzburg, Germany, where he worked on imaging diagnostics of solar cells. In 2004, he joined the Institute of Solid State Physics of the Leibniz University of Hannover as a Full Professor and became the Director of the Institute for Solar Energy Research in Hamelin (ISFH).



Jan Schmidt received the Diploma in physics from Clausthal Technical University, Clausthal-Zellerfeld, Germany, in 1993, and the Ph.D. degree in physics from the University of Hanover, Hanover, Germany, in 1998.

From 1998 to 2000, he worked as a Humboldt Fellow with Australian National University, Canberra, Australia, and from 2000 to 2001 as a Postdoctoral Researcher with the Institute of Physical Electronics, University of Stuttgart, Stuttgart, Germany. Since 2001, he is heading the Photovoltaics Materials Research activities with the Institute for Solar Energy Research Hamelin (ISFH), Hamelin, Germany. In parallel, he is a Full Professor with the Institute of Solid-State Physics, Leibniz University Hannover, Hannover. He has authored or coauthored more than 160 peer-reviewed journal papers and more than 120 conference papers in the fields of photovoltaics and semiconductor physics. His research interests include the development of novel solar cell concepts and fabrication processes, with focus on surface passivation and selective contacts, the development of novel characterization techniques for semiconductors and solar cells, and the analysis and manipulation of defects in mono and multicrystalline silicon materials.

Dr. Schmidt is Scientific Committee Member for several conferences (e.g., EUPVSEC, SiliconPV/nPV) and the Editor of the IEEE JOURNAL OF PHOTOVOLTAICS.